G.V.M. Gaias, J.-S. Ardaens
Design Challenges and Safety Concept for the AVANTI Experiment
Acta Astronautica, Vol. 123, 2016, p. 409-419
doi:10.1016/j.actaastro.2015.12.034

DESIGN CHALLENGES AND SAFETY CONCEPT FOR THE AVANTI EXPERIMENT

G. Gaias* and J.-S. Ardaens †

AVANTI is a formation-flight experiment involving two noncooperative satellites. After a brief overview of the challenges that experiment design and scenario induce, this paper presents the safety concept retained to guarantee the safety of the formation. The peculiarity of the proposed approach is that it does not rely on the continuous availability of tracking data of the client spacecraft but rather exploits the concept of passive safety of special relative trajectories. To this end, the formation safety criterion based on the minimum distance normal to the flight direction has been extended in order to be applicable also to drifting relative orbits, resulting from non-vanishing relative semi-major axis encountered during a rendezvous or produced by the action of the differential aerodynamic drag.

INTRODUCTION

The Autonomous Vision Approach Navigation and Target Identification (AVANTI) is a formation flight experiment currently in development at the German Space Operation Center. Its objective is to demonstrate the capability to perform autonomously rendezvous and receding approaches with respect to a noncooperative client satellite making use of vision-based angles-only measurements.[1] The experiment focuses on far- to mid-range inter-satellite separations (*i.e.*, from approximately 10 km to few hundreds of meters in the along-track direction) and the Berlin InfraRed Optical System (BIROS) satellite is employed as the active servicer spacecraft.

AVANTI is one of the secondary scientific experiments to be executed within the FireBird mission.[2] This is a small-scale scientific mission of the German Aerospace Center (DLR) for Earth observation and hot spot detection comprising a loose constellation of two satellites: TET-1, already launched in July 2012, and BIROS, scheduled for launch in 2016. In addition, BIROS will release in-orbit a picosatellite of the Technische Universität (TU) Berlin University, which, during AVANTI, will be used as noncooperative target.

In the recent years DLR performed the following autonomous formation control activities: the Spaceborne Autonomous Formation Flying Experiment (SAFE)[3] and the TanDEM-X Autonomous Formation Flying (TAFF) system.[4,5] Both these experiments are examples of cooperative scenarios, since the spacecraft communicated through an inter-satellite link. In addition, in order to achieve the required control accuracies, the estimation of the relative state exploited relative Global Positioning System (GPS) data from both the satellites.

Regarding vision-based noncooperative rendezvous scenarios, recent DLR flight activities involve the Formation Re-acquisition experiment[6] and the Advanced Rendezvous Demonstration

*Research Engineer, GSOC/Space Flight Technology, Münchner Str. 20, 82234 Wessling, Germany.
Corresponding Author: +49 (8153) 28-1769, gabriella.gaias@dlr.de
†Research Engineer, GSOC/Space Flight Technology, Münchner Str. 20, 82234 Wessling, Germany.

using Global Positioning System and Optical Navigation (ARGON) experiment.[7] Both of these campaigns took place within the Prototype Research Instruments and Space Mission Technology Advancement (PRISMA) mission, respectively at the end of the nominal mission timeline and during the extended phase.[8] The Formation Re-acquisition experiment was meant to re-establish a formation after the conclusion of the nominal mission. At that time, the two PRISMA spacecraft were separated by approximately 60 km, exceeding thus the inter-satellite link range. The experiment consisted of a ground-in-the-loop vision-based approach to decrease the separation to circa 4 km after one week. To that end, an early prototype of the angles-only relative navigation filter was developed, processing daily five-hour-long pictures slots of the target satellite taken by the vision-based sensor (VBS) embarked on the servicer satellite. The filter was initialized using two-line-elements (TLE) provided by the North American Aerospace Defense Command (NORAD). During the ARGON experiment, instead, an approach from 30 to 3 km was performed, making use of solely angles-only measurements coming from the VBS system. To that end, a dedicated ground-based flight dynamics system has been developed for routine processing of the camera images collected on-board, for estimation of the relative orbit of the servicer with respect to the client vehicle, and for conducting the maneuver planning. Finally, the availability of independent and precise navigation information from carrier-phase differential GPS techniques has been exploited *post-facto* to properly evaluate the achieved performance after the conclusion of the technology demonstration.

Based on the experience gained with the aforementioned ground-based guidance navigation and control (GNC) system, the development of the AVANTI experiment aims at enhancing further the DLR expertise in the field of noncooperative rendezvous. The major contribution of AVANTI lies in passing from a ground-based approach to fully autonomous onboard operations. Nevertheless, besides this change of paradigm, several other issues related to the specific orbit scenario, to the hosting platform, and to communication and ground segment requirements pose different challenges to the implementation of the AVANTI GNC software. As an example, the model of the relative motion between satellites flying in near-circular low-Earth-orbits employed in the previous formation flying missions has been improved to reflect the non-negligible effects of the differential aerodynamic drag.[9] Moreover, the vision-based navigation system has been designed to cope with the eclipses that occur all year long and impact the distribution of the available optical measurements.[10] Regarding platform and ground segments requirements, the guidance module of AVANTI is able to allow the definition of time slots where no maneuver activities shall occur (*e.g.*, to avoid interaction between maneuvers and payload or to account for the time necessary to point the single-direction thruster system into the desired direction). Furthermore, the guidance module is also in charge of the selection in real-time of the most appropriate attitude mode (*e.g.*, picture data take, power and thermal needs, communication pointing requirements).[11]

In addition to the aforementioned design challenges, AVANTI is truly noncooperative, because no absolute tracking data of the picosatellite will be available during the experiment execution. Consequently, in order to guarantee the safety of the whole mission, a specific concept has been developed, mainly based on passive safety and especially capable of accounting for long term effects of the differential drag, and for maneuver execution errors. In this framework, this paper addresses the solution implemented to achieve a safe design for the autonomous GNC software during its operational life.

COLLISION AVOIDANCE FOR THE FORMATION

During the execution of AVANTI, FireBird becomes a formation flying mission. Thus special attention is required to perform safe operations of two spacecraft close to each other, in the presence of navigation uncertainties and maneuver execution errors. In the case of AVANTI, this formation collision avoidance task is even more critical since noncooperative satellites are involved and operation phases with a high level of autonomy are foreseen.

Former formation flying missions employed collision avoidance approaches either based on passively safe relative trajectories, or on maneuver reaction strategies which relied on the continuous availability of an accurate and independent source of navigation data, or on the combination of the two methodologies. The passive safety technique is inspired by the co-location of geostationary satellites sharing the same longitude window.[12] Afterwards, the concept of establishing relative trajectories characterized by (anti-)parallel relative eccentricity and inclination vectors has been demonstrated in low-Earth orbit to carry out the safe switching of the GRACE formation[13] The formalization of this methodology applied to formation flying missions is provided in Reference 14. Examples of in-flight utilization are the SAFE experiment,[3] and the TanDEM-X formation.[15] Finally, the rendezvous profile pursued during ARGON was designed to have a spiraling relative motion to achieve a passively safe final relative orbit.[7]

Among its formation flying demonstrations, the PRISMA mission performed some experiments that required the use of relative orbits which were not naturally safe (*i.e.*, that could result in collision in case of loss of the nominal orbit control functionality). The collision avoidance strategy retained in PRISMA is described in Reference 16. According to it, a collision monitoring module exploited the GPS-based position information of the two satellites to propagate the 3-D uncertainty ellipsoid of the relative position vector. Then, in case of overlapping of the n-sigma relative ellipsoid with a r-sphere centered on the origin of the local orbital frame, the separation guidance task was triggered to compute autonomously onboard the orbit correction maneuvers that met certain criteria. It is emphasized that, during the execution of ARGON, although the experimenters did not know the *true* satellites' absolute positions, the onboard collision avoidance module was active and the ground-segment operation team was constantly monitoring the GPS-based reference absolute orbits.

The starting point to design a collision avoidance strategy for AVANTI is the analysis of the available navigation data sources, for both satellites, with their related accuracies. BIROS embarks a DLR Phoenix GPS receiver and an Onboard Navigation System (ONS) module processing the GPS measurements to provide onboard absolute navigation with a 20 m accuracy. Although BEESAT-4 also embarks a Phoenix GPS receiver,[17] the picosatellite itself is a third-party experimental activity and operationally it is ruled out that one technology demonstration may depend on another one to accomplish its objectives. Consequently, BIROS and BEESAT-4 will not communicate during formation flying activities. Alternative data sources to perform the absolute orbit determination of the picosatellite could be TLE and radar tracking observations. Nevertheless, neither of these options can support the design of a collision avoidance strategy within the mission scenario of AVANTI. TLE, in fact, if available at all, are typically accurate only to 1.5 km in the along-track direction. The radar tracking facility foreseen within FireBird to support the in-orbit release of the picosatellite requires a minimum inter-satellite distance of 5 km in order to distinguish the signals from the two spacecraft. In this case, an estimation of the achievable orbit determination performance is provided in Reference 18.

In the absence of absolute tracking data of the picosatellite, the only source of navigation infor-

mation is provided by the star tracker used as a camera sensor during AVANTI. As a result, the monitoring and performance assessment of the onboard navigation solution can only be performed by reprocessing on-ground the vision-based measurements collected in-flight. In this case, in fact, the relative orbit determination process becomes man-in-the-loop and can include better estimates of the executed maneuvers, coming from the BIROS Precise Orbit Determination (POD) products. However, this comes at the cost of a longer reaction time, directly driven by the frequency of ground contacts.

Safety concept design for AVANTI

The safety concept retained to mitigate the collision hazard during the execution of the AVANTI experiment does not rely on the continuous availability of picosatellite tracking data. It is mainly based on passive safety, completed by additional safety measures:

1. The relative trajectory must always be characterized by a safe (anti-)parallel configuration of the relative eccentricity and inclination vectors.

2. *Onboard preventive action*: each maneuver command generated by AVANTI is forwarded to the AOCS system and executed only if the post-maneuver relative orbit is considered to be safe at least during the 24 hours following the evaluation time.

3. *Long-term reaction*: any required orbit correction maneuver (*e.g.*, via generation of new telecommands for AVANTI or directly commanded to BIROS) is assessed on-ground, based on the analysis of the retrieved telemetry.

The onboard preventive action is performed by the Onboard Safety Monitoring (OSM) application, which is explained in the next section.

After the in-orbit release of the picosatellite from BIROS, the AVANTI experiment starts as soon as the experiment initial conditions are achieved. This task is purely ground-based and performed by the Flight Dynamics Services (FDS) division of the German Space Operations Center (GSOC) with the support of radar tracking campaigns. Together, the picosatellite ejection strategy and the orbit correction maneuvers performed after the first on-ground picosatellite orbit determination ensure that the relative orbit, at the start of the experiment, is passively safe.[19]

After the activation of AVANTI, the guidance module ensures that the safe phasing of the relative eccentricity and inclination vectors is kept throughout all the maneuvers required for the rendezvous.[11] Therefore, it becomes possible to always maintain a desired minimum distance in the radial-normal plane by simply avoiding too small relative orbits or rapid changes of relative mean longitude (since a large relative semi-major axis induces a large shift in the radial direction). Both these conditions are controllable via telecommand. Thus the maneuver planning carried out by AVANTI preserves the passive safety of the relative trajectory.

During all the formation flying phases the picosatellite precedes BIROS in flight direction, as BEESAT-4 presents a larger impact area to mass ratio in all the attitude configurations foreseen for AVANTI. Consequently, the effect of the differential aerodynamic drag produces a natural increase of the inter-satellite separation over time. Thus, whenever a rendezvous is interrupted, BIROS will naturally start first reducing then reversing its drift, ultimately towards the evaporation of the formation.

To conclude, the basic idea of the proposed safety concept is to keep the formation in configurations that, even in case of interruptions of the ongoing maneuver plan, will not result in dangerous conditions for at least 24 hours following the break. This allows an intervention from ground to evaluate more appropriate countermeasures. The AVANTI SW implements several integrity checks in order to detect possible anomalous behaviors. Nevertheless, in the improbable case that a dangerous maneuver is generated by the guidance module, the supervision of the OSM application prevents its execution. The function and evaluation criterion adopted by this safety monitoring module are addressed in the next section.

THE ONBOARD SAFETY MONITORING MODULE

The goal of the OSM module is to supervise the safety of the BEESAT-4 – BIROS formation during the execution of the AVANTI experiment. To this end OSM exploits a *reference* relative trajectory which is obtained by propagating in time an initial relative state provided from ground. Within the space segment, this reference trajectory represents the best available knowledge of the true relative state.

As depicted in Figure 1, OSM is implemented in the BIROS onboard computer and runs independently from AVANTI. OSM receives from ground via telecommand the value and variance of the best estimation of the relative state at a certain time t_0, which are obtained from the on-ground reprocessing of the latest available telemetry. Starting from these initial conditions, OSM internally propagates the state and its variance-covariance matrix until a prediction time t_p (*i.e.*, the current time plus 24 hours) including the list of maneuvers executed since the last refresh time t_0. The so obtained predicted state distribution is used to assess the safety of the formation. As soon as AVANTI computes a new orbit maneuver command, it calls OSM, which evaluates the safety of the action and provides feed-back to AVANTI (dashed gray arrows in Figure 1). As a result, a maneuver command is forwarded to the AOCS system for execution only if the post-maneuver relative orbit at the prediction time is considered safe.

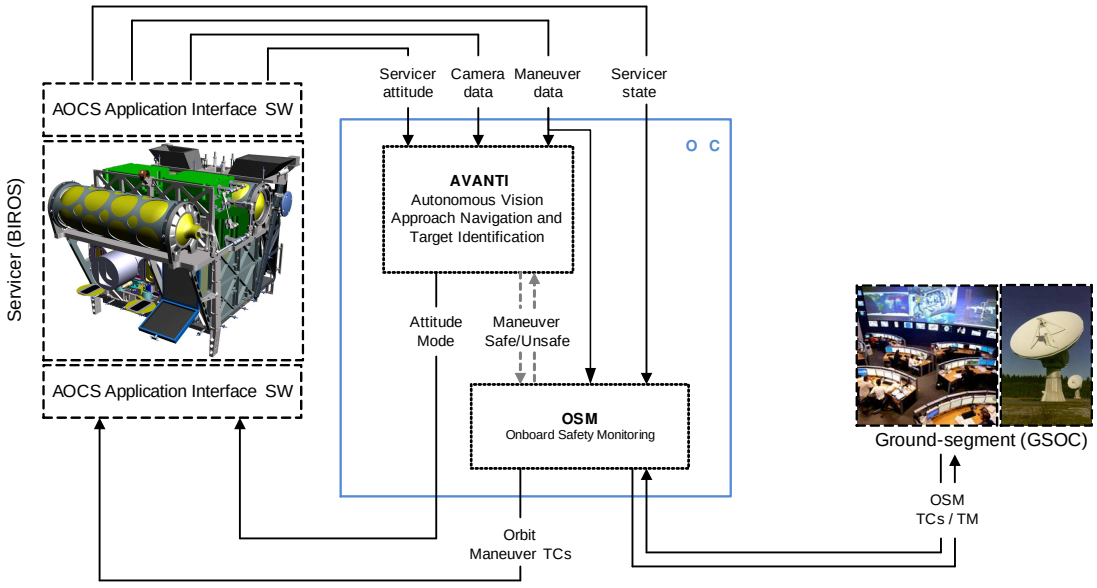

Figure 1. OSM architecture and interfaces to space and ground segments.

Given the distribution of the relative state at the prediction time, the criterion to assess the safety of the formation is expressed by:

$$\delta\bar{r}_{\mathrm{RN}}^{\mathrm{min}} - 3\sigma_{\delta r_{\mathrm{RN}}^{\mathrm{min}}} > M \tag{1}$$

where $\delta r_{\mathrm{RN}}^{\mathrm{min}}$ is the minimum distance between the one-orbit projection on the radial-normal (R-N) plane of the local orbital frame centered on BIROS and its origin. The symbols $(\bar{\bullet}, \sigma_{\bullet})$ identify expected value and standard deviation of the minimum RN distance distribution. Finally, M is a safety margin representable as a circle of radius M around the origin of the R-N plane.

The criterion of Eq. (1) provides a correct assessment of the safety properties of the *true* relative orbit only if the algorithms implemented in OSM are able to fulfill the following capabilities:

1. precise long-term propagation of the relative state able to reflect the long-term effects of differential drag and maneuver execution errors;
2. accurate computation of the minimum RN distance at every time;
3. accurate estimation of expected value and standard deviation of the minimum RN distance distribution;
4. numerical verification that no elements of the *true* minimum RN distance distribution which are unsafe are incorrectly judged as safe when using the approximated quantities.

The next subsections address these specific topics.

Relative motion propagation

The relative motion is described by the following set of dimensionless relative orbital elements (ROEs):[9]

$$\delta\boldsymbol{\alpha} = f(\boldsymbol{\alpha}, a_{\mathrm{c}}, i_{\mathrm{c}}) - f(\boldsymbol{\alpha}_{\mathrm{c}}, a_{\mathrm{c}}, i_{\mathrm{c}}) = \left(\begin{array}{cccccc} \delta a, & \delta\lambda, & \delta e_x, & \delta e_y, & \delta i_x, & \delta i_y \end{array} \right)^{\mathrm{T}} \tag{2}$$

where

$$f(\boldsymbol{\alpha}, a_{\mathrm{c}}, i_{\mathrm{c}}) = \begin{pmatrix} a/a_{\mathrm{c}} \\ u + \Omega\cos i_{\mathrm{c}} \\ e\cos\omega \\ e\sin\omega \\ i \\ \Omega\sin i_{\mathrm{c}} \end{pmatrix}, \tag{3}$$

$\boldsymbol{\alpha} = (a, e, i, \omega, \Omega, u)^{\mathrm{T}}$ is the set of classical Keplerian orbital elements, u is the spacecraft mean argument of latitude, and the subscript "c" labels the BIROS satellite. The Cartesian and polar expressions for the relative eccentricity and inclination vectors are:

$$\delta\mathbf{e} = \begin{pmatrix} \delta e_x \\ \delta e_y \end{pmatrix} = \delta e \begin{pmatrix} \cos\varphi \\ \sin\varphi \end{pmatrix} \qquad \delta\mathbf{i} = \begin{pmatrix} \delta i_x \\ \delta i_y \end{pmatrix} = \delta i \begin{pmatrix} \cos\theta \\ \sin\theta \end{pmatrix} \tag{4}$$

with φ denoting the perigee and θ the ascending node of the relative orbit as depicted in Figure 2. In order to develop an accurate and complete model for the relative motion in near-circular low-Earth-orbits, the dimensional relative state expressed by the ROE set is augmented by three constant additional parameters, characterized by a straightforward geometrical interpretation:[9]

$$\mathbf{x} = (a\delta\boldsymbol{\alpha}, a\delta\dot{a}, a\delta\dot{e}_x, a\delta\dot{e}_y)^{\mathrm{T}} \tag{5}$$

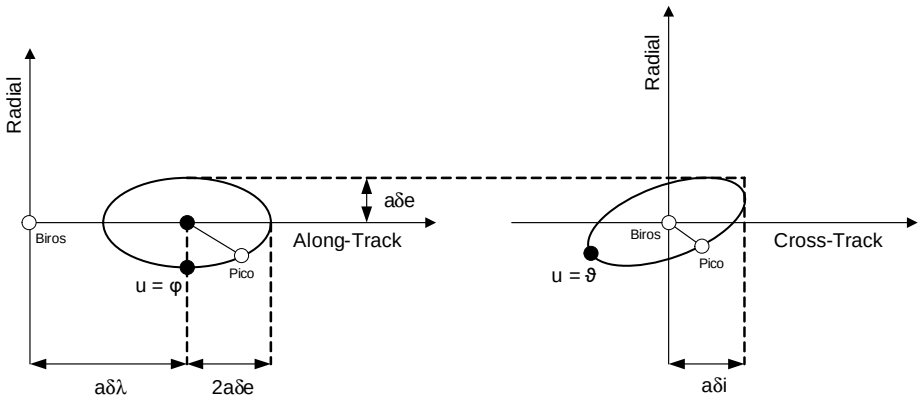

Figure 2. Geometrical representation of the ROEs defined in Eqs. (2) and (4).

Note that the subscript "c" is no longer marked. The first additional parameter is the time derivative of the relative semi-major axis $a\delta\dot{a}$. The remaining two are the time derivatives respectively of the x and y components of the relative eccentricity vector. These additional parameters make it possible to describe the mean time variations of the in-plane ROEs when subject to time-varying differential aerodynamic drag. Accordingly, the state transition matrix for the relative motion in near-circular low-Earth-orbits expressed as function of the complete relative state $\mathbf{x}$ is written as:

$$\mathbf{x}(t) = \mathbf{\Phi}(t,t_0)\,\mathbf{x}(t_0) = \begin{bmatrix} \mathbf{\Phi}_{\text{HCW}}(t,t_0) + \mathbf{\Phi}_{\text{J2}}(t,t_0) & \tilde{\mathbf{\Phi}}_{\text{d-drag}}(t,t_0) \\ \mathbf{O}_{3\times 6} & \mathbf{I}_{3\times 3} \end{bmatrix} \mathbf{x}_0 \tag{6}$$

where "HCW" denotes the Hill-Clohessy-Wiltshire contribution, "J2" the mean effects produced by the Earth's oblateness perturbation, and $\tilde{\mathbf{\Phi}}_{\text{d-drag}}$ collects the joint effect of differential aerodynamic drag and J_2, whose detailed expressions are provided in Reference 9. Despite its simplicity, the model of Eq. (6) accounts for all the dominant perturbations that occur in the low-Earth-orbit environment. Moreover, since the motion is parametrized through relative orbital elements, the limited range validity of the inter-satellite distance, typical of Cartesian formulations, are overcome. Finally, the employed relative motion model is fully linear in the initial state $\mathbf{x}_0$, which is very beneficial for the onboard implementation.

The relative motion propagation implemented in OSM, starting from the latest best estimate of the expected value and its variance-covariance matrix $(\bar{\mathbf{x}}_0, \mathbf{P}_0)$, is given by:

$$\begin{cases} \bar{\mathbf{x}}(t) &= \mathbf{\Phi}(t,t_0)\,\bar{\mathbf{x}}_0 + \displaystyle\sum_{i=1}^{n} \mathbf{\Phi}(t,t_i)\,\mathbf{B}(t_i)\delta\mathbf{v}_i \\ \mathbf{P}(t) &= \mathbf{\Phi}(t,t_0)\,\mathbf{P}_0\,\mathbf{\Phi}^{\mathrm{T}}(t,t_0) + \displaystyle\sum_{i=1}^{n} \mathbf{\Phi}(t,t_i)\,\mathbf{B}(t_i)\left[\sigma^2_{\delta v,i}\,\mathbf{I}_{3\times 3}\right]\left(\mathbf{\Phi}(t,t_i)\,\mathbf{B}(t_i)\right)^{\mathrm{T}} \end{cases} \tag{7}$$

where $\mathbf{B}$ is the matrix of partial derivatives of $\mathbf{x}$ with respect to the velocity change expressed in the RTN frame and n is the number of maneuvers carried out between t_0 and the propagation time t. In order to write the terms $\mathbf{\Phi}(t,t_0)$ and $\mathbf{\Phi}(t,t_i)$, the property presented in Eq. (11) of Reference 11, which remains valid also for the more comprehensive state transition matrix of Eq. (6), is used. Regarding the relative eccentricity vector portion of the matrix, the negligible numerical approximation introduced in Eq. (15) of Reference 11 is employed. Since in Eq. (7) the maneuvers

are included as impulsive delta-vs, the standard deviation parameter $\sigma_{\delta v}$ has to collect the effect of the maneuver execution errors together with the thruster system modeling error. Regarding its numerical value, $\sigma_{\delta v}$ can be defined via telecommand.

Computation of the minimum RN distance

The minimum RN distance associated with a relative orbit as function of time can be defined by mapping the $a\delta\boldsymbol{\alpha}(t)$ ROE set in the RN plane with the mean argument of latitude u spanning one orbit according to:

$$\delta r_{\text{RN}}^{\text{min}} = \min_{u\in[0,2\pi)} \sqrt{\left(a\delta i\, \sin(u-\theta)\right)^2 + \left(a\delta a - a\delta e\, \cos(u-\theta-\phi)\right)^2} \tag{8}$$

where $\phi = \varphi - \theta$ is the phasing of the relative eccentricity and inclination vectors.

In order to select the final relative orbit for the ARGON experiment,[7] the following approximation of the solution of Eq. (8) has been employed:

$$\delta r_{\text{RN}}^{\text{min, approx}} = \begin{cases} |\,|a\delta a| - a\delta e\,| & \text{, if } sign(a\delta a + a\delta e) = sign(a\delta a - a\delta e) \\ \min\{a\delta i, |\,|a\delta a| - a\delta e\,|\} & \text{, other cases} \end{cases} \tag{9}$$

which provides the correct result only in the case of (anti-)parallel configurations (*i.e.*, $\phi = 0 + k\pi$) and bounded relative orbits (*i.e.*, $a\delta a = 0$). As soon as $\phi \neq 0 + k\pi$, this approximation reveals itself to be too conservative in the presence of large drifts (*i.e.*, $|a\delta a| > a\delta e$) and too optimistic for small values of the relative semi-major axis. Since OSM propagates the relative motion over long periods of time, the conditions on ϕ and $a\delta a$ can never be respected due to the effects of the orbital perturbations. In addition, an optimistic estimation of the minimum RN distance, as it occurs in the typical AVANTI scenario of lengthy rendezvous towards the client, constitutes a danger for the mission, since the *true* separation might be significantly smaller than the approximated one.

In the case of the (anti-)parallel configuration, the solution of Eq. (8) for drifting relative orbits can be formulated as:

$$\delta r_{\text{RN}}^{\text{min, par}} = \min_i \{\delta r_{\text{RN}}(\beta_i)\} \tag{10}$$

where δr_{RN} is the RN distance function computed in the points β:

$$\begin{aligned} &\beta = u - \theta = \{0, \pi\} \\ &\beta = u - \theta = \arccos((\mp\delta a\, \delta e)/(\delta i^2 - \delta e^2)) \end{aligned} \tag{11}$$

which are the stationary points of the square of Eq. (8) (*i.e.*, δr_{RN}^2). Finally, the solution of Eq. (8)

that covers all the possible typologies of relative orbits can be expressed as:

$$\delta r_{\text{RN}}^{\text{min}} = \begin{cases} |a\delta a| & \text{, if } a\delta e = 0 \\ \delta r_{\text{RN}}^{\text{min, par}} & \text{, if } |\sin(\phi)| = 0 \\ 0 & \text{, if } a\delta a = 0 \text{ and } |\cos(\phi)| = 0 \\ 0 & \text{, if } a\delta i = 0 \text{ and} \\ & \quad \text{sign}(a\delta a + a\delta e) \neq \text{sign}(a\delta a - a\delta e) \\ |\,|a\delta a| - a\delta e\,| & \text{, if } a\delta i = 0 \text{ and} \\ & \quad \text{sign}(a\delta a + a\delta e) = \text{sign}(a\delta a - a\delta e) \\ \left| a\delta a \sin\left(\arctan\left(\dfrac{a\delta i}{a\delta e}\right)\right)\right| & \text{, if } |\cos(\phi)| = 0 \text{ and } |g| \leq a\delta i \\ \sqrt{(a\delta i)^2 + (|a\delta a| - a\delta e)^2} & \text{, if } |\cos(\phi)| = 0 \text{ and } |g| > a\delta i \\ \min\left\{\delta r_{\text{RN}}\left(\frac{\gamma}{2}\right), \delta r_{\text{RN}}\left(\frac{\gamma+\pi}{2}\right)\right\} & \text{, if } a\delta a = 0 \text{ and } |\cos(\phi)| \neq 0 \\ \delta r_{\text{RN}}(z^*) & \text{, other cases} \end{cases} \tag{12}$$

with

$$g = \frac{|a\delta a|\,\delta e\,\delta i}{(\delta e^2 + \delta i^2)} \qquad \gamma = \arctan\left(-\frac{\delta e^2 \sin(2\phi)}{\delta i^2 - \delta e^2 \cos(2\phi)}\right) \tag{13}$$

and z^* a real root of the 4$^{\text{th}}$ order polynomial in $z = \tan((u-\theta)/2)$ with coefficients:

$$\begin{aligned} c_4 &= 2a\delta e\,(a\delta e\cos\phi + a\delta a)\sin\phi \\ c_3 &= +4(a\delta e)^2\left(\cos^2\phi - \sin^2\phi\right) + 4a\delta a\, a\delta e\cos\phi - 4(a\delta i)^2 \\ c_2 &= -6(a\delta e)^2\sin(2\phi) \\ c_1 &= -4(a\delta e)^2\left(\cos^2\phi - \sin^2\phi\right) + 4a\delta a\, a\delta e\cos\phi + 4(a\delta i)^2 \\ c_0 &= 2a\delta e\,(a\delta e\cos\phi - a\delta a)\sin\phi \end{aligned} \tag{14}$$

In OSM the minimum RN distance is computed through Eq. (12), thus avoiding introducing approximation errors at this stage of the algorithm, at a very low computational cost.

Approximation of the minimum RN distance distribution

The formation-flight problem of satellites in near-circular orbits, with the inter-satellite ranges foreseen for AVANTI and a state variable set expressed in ROEs, turns out to be suitable for accurate propagation through the linear system of equations Eq. (7). The initial distribution of the relative state $(\bar{\mathbf{x}}_0, \mathbf{P}_0)$ is the output of the on-ground vision-based navigation filter and it is assumed to be Gaussian. Consequently, the relative state distribution at a later time $(\bar{\mathbf{x}}(t), \mathbf{P}(t))$ remains Gaussian, as linear transformations preserve the moments of a distribution.

The minimum RN distance over time is a nonlinear function of the elements ($a\delta a$, $a\delta e_x$, $a\delta e_y$, $a\delta i_x$, $a\delta i_y$) and is expressed in Eq. (12). According to the evaluation criterion of OSM, in order to assess the safety property of a trajectory the expected value $\delta\bar{r}_{\text{RN}}^{\text{min}}$ and standard deviation $\sigma_{\delta r_{\text{RN}}^{\text{min}}}$ of the minimum RN distance distribution need to be computed.

Among the available methods to propagate means and covariances through nonlinear transformations, approaches based on linearization are discarded, since they provide accurate results only when

Eq. (12) can be well approximated by a linear function and the computation of its Jacobian matrix is difficult and potentially error-prone for the implementation in the flight software. The method selected for the OSM application case, instead, is based on the unscented transformation (UT). This framework, in fact, offers a simple mechanism to compute the first two moments of a distribution after a nonlinear transformation, achieving a projected mean and covariance correct to the second order.[20] The mechanism of computation does not rely on the calculation of the derivatives of $\delta r_{\text{RN}}^{\text{min}}$ with respect to the relative state components. Finally, given the dimension of the problem under treatment (*i.e.*, the minimum RN distance is a function of only 5 components of the relative state), the number of required sigma points to approximate the transformed distribution is compliant with the computational resources available onboard.

Considering that the distribution of the relative state over time is Gaussian, the extended-symmetric-set of sigma points described in Reference 20 is employed. Accordingly, the following 11 $\mathbf{z}$ points are used for representing the distribution of the relative state:

$$\begin{aligned} \mathbf{z}^{(0)} &= \bar{\mathbf{x}} & W^{(0)} \\ \mathbf{z}^{(i)} &= \bar{\mathbf{x}} + \left(\sqrt{\frac{N}{1-W_0}\mathbf{P}}\right)_i & W^{(i)} = \frac{1-W_0}{2N} \\ \mathbf{z}^{(i+N)} &= \bar{\mathbf{x}} - \left(\sqrt{\frac{N}{1-W_0}\mathbf{P}}\right)_i & W^{(i+N)} = \frac{1-W_0}{2N} \end{aligned} \tag{15}$$

where $N = 5$ is the dimension of the state, i spans from 1 to N, the quantity $(\bullet)_i$ is the ith column of the matrix square root of $N/(1-W_0)\mathbf{P}$, and $W^{(\bullet)}$ are the weights associated with the sigma points. The value $W^{(0)}$ is a parameter $\in (-1, 1)$ that weights the point added to the symmetric set, in order to reflect some aspects of the higher moments of the sigma points distribution, without affecting the values of the first two. As a result, the expected value and variance of the minimum RN distance distribution are obtained from:

$$\begin{aligned} \delta\bar{r}_{\text{RN}}^{\text{min}} &= y = \sum_{i=0}^{2N} W^{(i)}\, \delta r_{\text{RN}}^{\text{min}}\left(\mathbf{z}^{(i)}\right) \\ \sigma^2_{\delta r_{\text{RN}}^{\text{min}}} &= P_y = \sum_{i=0}^{2N} W^{(i)}\, \left(\delta r_{\text{RN}}^{\text{min}}\left(\mathbf{z}^{(i)}\right) - y\right)^2 \end{aligned} \tag{16}$$

Numerical validation of the implemented algorithms

The first step of the numerical validation process consists of assessing how accurate the estimation of the minimum RN distance distribution computed through Eq. (16) can be. To this end, various configurations are investigated, characterized by different mean relative states $\bar{\mathbf{x}}$ and a fixed variance-covariance matrix with uncorrelated uncertainties and the following diagonal:

$$\sigma^{\mathbf{2}}_{\mathbf{x}} = (10^2, -, 20^2, 20^2, 20^2, 20^2, -, -, -) \tag{17}$$

where the symbol "-" has been used for the components of the relative state that have no role in the computation of the RN distance as defined in Eq. (8).

Figures 3(a) and 3(b) provide two examples of minimum RN distance distributions. The *true* profile is obtained by evaluating Eq. (12) 10^5 times, once for each element of the $(\bar{\mathbf{x}}, \mathbf{P})$ population.

The dashed vertical line identifies the mean value of the true distribution. The solid vertical lines, instead, delimit the true $\delta\bar{r}_{\mathrm{RN}}^{\mathrm{min}} \pm 3\sigma_{\delta r_{\mathrm{RN}}^{\mathrm{min}}}$ (when greater than zero). In the legend, the values of skewness and kurtosis difference with respect to 3 (*i.e.*, the value for a Gaussian distribution) are also reported. When the minimum RN distance values lay far enough from zero, the distribution remains almost Gaussian (Figure 3(a)). On the contrary, by approaching the origin, the shape can become extremely skewed (Figure 3(b)).

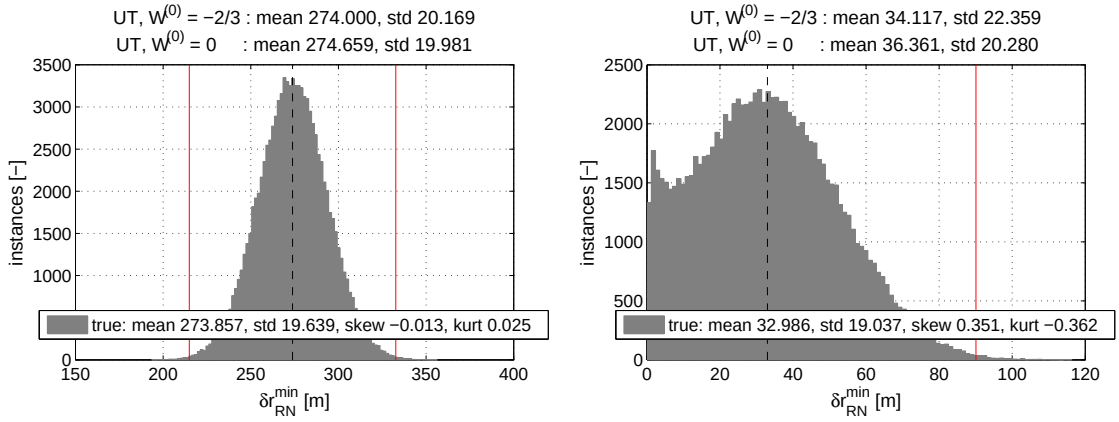

(a) x=(−50,−,480,0,280,0,−,−,−)m (b) x=(0,−,40,10,400,0,−,−,−)m

Figure 3. Examples of minimum RN distance distributions.

In the title of each view the approximated values of mean and standard deviations are reported, for two possible $W^{(0)}$ namely: $-2/3$ and 0. The first option weights the additional point to match up to some of the fourth-order moments the initial Gaussian distribution and its numerical value is computed as $W^{(0)} = 1 - N/3$.[20] The second choice corresponds to the purely symmetrical set.

In order to select a sigma-point family between the two already proposed, an extensive investigation of all possible variable combinations within the relative orbits domain applicable during AVANTI has been performed. To reduce the number of evaluations, the symmetry of the RN distance expression suggested to employ as variables the functions of the 5 components of $\mathbf{x}$ reported in Table 1, where $a\delta e$ and $a\delta i$ are the dimensional magnitudes of relative eccentricity and inclination vectors in agreement with Eq. (4). Boundaries and graduation are also indicated.

Table 1. Investigated combinations of relative orbits.

Variable	Unit	Min	Max	Step
$a\delta a$	m	-250	0	50
$a\delta e$	m	0	600	40
$a\delta i$	m	0	600	40
ϕ	deg	0	90	5

Each combination of variables is taken as a mean relative state $\bar{\mathbf{x}}$ of accuracy $\mathbf{P}$, to which a population of 1000 elements is associated in order to compute the true minimum RN distance distribution. These constitute the reference when comparing the moments estimated through Eq. (16) for the two $W^{(0)}$ weights. As a result, the estimation errors for both mean value y and standard deviation $\sqrt{P_y}$ are shown in Figure 4. From a visual point of view the $W^{(0)} = 0$ option (marked in black) tends to achieve a lower error in the majority of the cases. It is emphasized that in this

extensive research no combinations are discarded, even if the corresponding relative state identifies a relative trajectory obviously unsafe, whose true distribution presents a distorted profile, therefore difficult to be estimated.

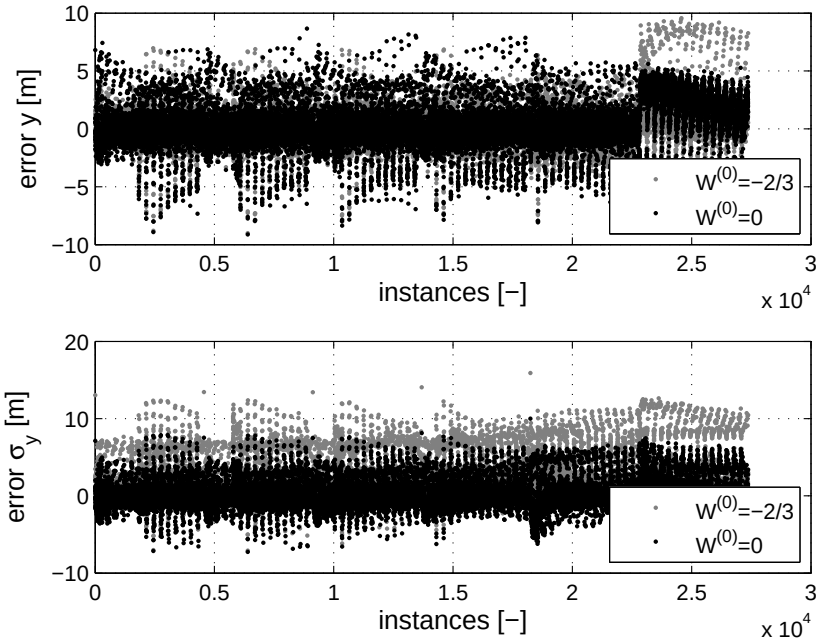

Figure 4. Accuracy of the estimation of the minimum RN distribution for all the cases defined in Table 1.

Having assessed the obtainable accuracy in estimating the minimum RN distance distribution, the following approach was chosen to implement the safety criterion. The margin M of Eq. (1) is set equal to 15 m, to accommodate the global effect of the estimation errors in mean and standard deviation. Moreover, in order to avoid useless computations and, at the same time, to discard error-prone instances, a threshold $R = 40$ meters is introduced. Accordingly, whenever the evaluation of the $\delta r_{\mathrm{RN}}^{\mathrm{min}}$ function in $\bar{x}$ is minor equal to the R threshold, the relative orbit is straightaway declared as unsafe. The boundaries that delimit the estimated minimum RN distance distribution become:

$$\left[\max\left\{y - 3\sqrt{P_y} - M, 0\right\}, \qquad y + 3\sqrt{P_y} + M\right] \tag{18}$$

Both the settings M and R are controllable via telecommand.

In order to verify the proposed approach, all the instances of Table 1 were reprocessed, achieving the following results:

1. no instances judged unsafe according to the true distribution (*i.e.*, $\delta\bar{r}_{\mathrm{RN}}^{\mathrm{min}\ \mathrm{true}} - 3\ \sigma_{\delta r_{\mathrm{RN}}^{\mathrm{min}}}{}^{\mathrm{true}} \leq 0$) were considered safe by the criterion of Eq. (1);

2. the instances judged safe according to the true distribution but (conservatively) unsafe by OSM present the true lower limits depicted in Figure 5, left view. As expected, the majority of the cases accumulate in the margin M band. The number of these instances conservatively judged as unsafe amounts to 2018, which corresponds to $\approx 7.4\%$ of the total investigated

cases. Note that the x-axes of Figures 4 and 5 span the same interval, since the position index is considered, rather than the incremental number of instances;

3. for all the instances judged safe according to both true and estimated distributions, the percentage of elements of the true population that lay in the estimated bounds is at minimum 99.6% (see Figure 5, right view). Note that the granularity of 0.1% is due to having taken populations of 1000 elements for each investigated case.

Together these results produce the numerical evidence that the approach implemented in OSM provides a reliable evaluation of the safety properties of the relative trajectory.

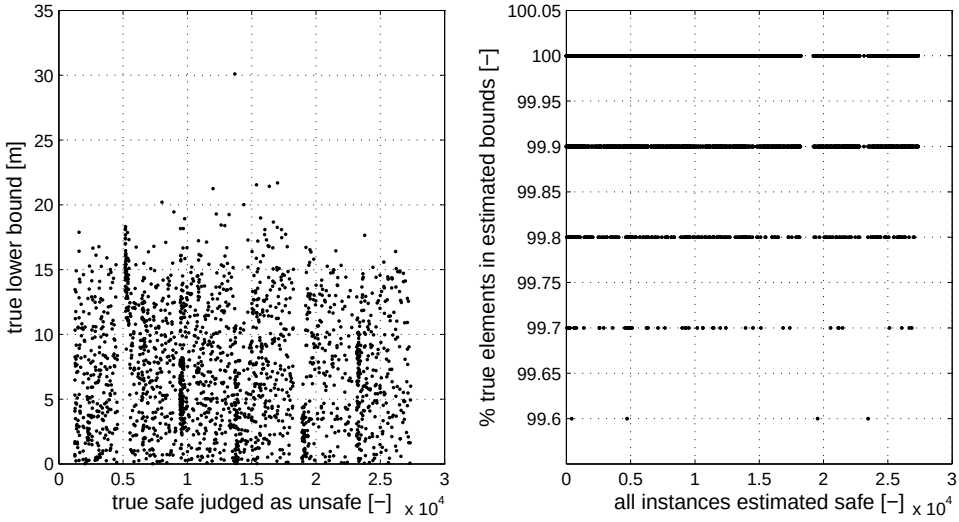

Figure 5. Figures of merit to verify the validity of the OSM approach.

EXAMPLE OF FUNCTIONING OF THE SOFTWARE

In order to provide an example of the output of the OSM software, the same scenario discussed in Reference 1 has been considered. It mimics the initial phases of the AVANTI experiment, immediately after that the FDS achieves the experiment initial conditions at the completion of the picosatellite in-orbit injection. Accordingly, an approach reducing by 4 km the relative mean longitude to the client is accomplished in approximately 25 hours.

Figure 6 depicts the interaction between the AVANTI and OSM applications. OSM is constantly monitoring the formation: the "isSafeFuture" flag collects the result of the safety check at the prediction time for every call. As soon as the AVANTI guidance reaches the "Command man" internal state, it calls OSM (see "ManEvaluated") and receives an answer back. In the simulation no safety violations happened, therefore MAP expects that the command will be transmitted to the thruster system and continues to "Wait end man". Note that the upper plot of Figure 6 also appears as Figure 9 of Reference 1.

Figure 7 shows the error over time that the internal propagation function of OSM commits with respect to the true state, here available from the simulation environment. The ROE portion of the relative state is depicted and the error is computed as the difference between propagated and true

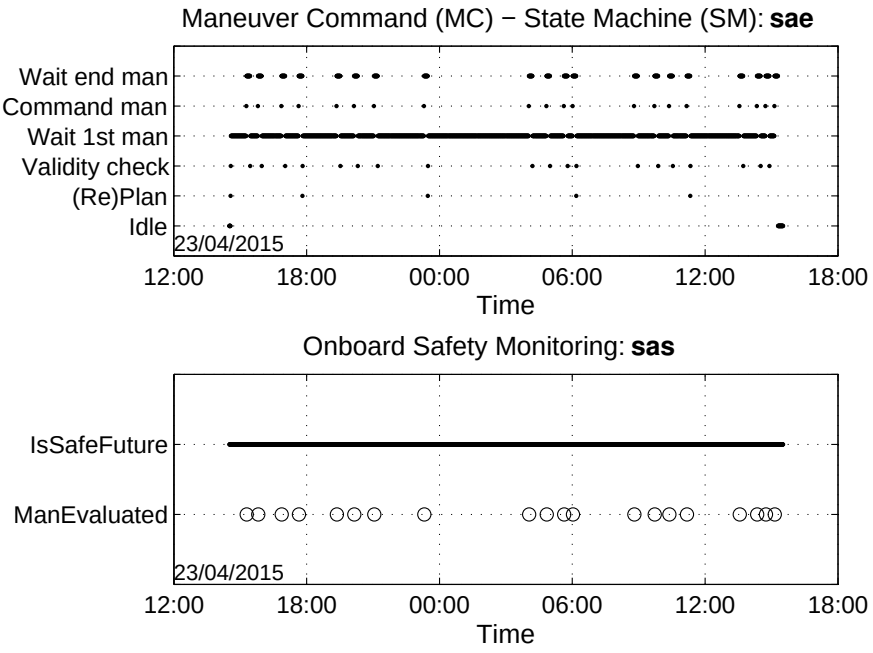

Figure 6. The preventive action of OSM.

values. Sparse points appear when maneuvers are performed. OSM, introduces instantaneous delta-vs, whereas the thruster system requires a few minutes of burn time to provide the equivalent delta-v. Vertical solid lines mark the reception times of telecommands from ground, here occurring every 12 hours. Consequently, the relative state is (re-)initialized with an accuracy corresponding to a standard deviation σ_{ROE} of $(5, 80, 15, 15, 15, 15)$ meters. Figure 7 shows that the relative motion model of Eqs. (6) and (7) supplies an accurate estimation even for long periods of time after the last update of the initial conditions.

Finally, Figures 8 and 9 provide a visualization of the safety concept approach based on minimum RN distance, respectively over time and in the RN plane. In Figure 8, the RN distance of the true trajectory at the time in which OSM is called is plotted in gray. Given the geometry of the relative orbit (see its projection on the RN plane in Figure 9), it presents a periodical pattern with local and global minimum and maximum extrema. The approach of exploiting the minimum RN distance as defined in Eq. (8) and computed through Eq. (12), instead, determines at every time the global minimum of the corresponding relative orbit. And y, marked in bold black, is the estimated expected value of the distribution that the minimum RN distance can present due to the errors affecting the relative state.

Since the proposed approach is based on the one-orbit minimum RN distance, it provides an intrinsically conservative evaluation of the relative trajectory safety. In addition, the $\delta r_{\text{RN}}^{\text{min}}$ function varies smoothly with the passing of the time, driven from the behavior of the solution of the relative motion expressed in ROEs. A minimum RN distance jump can only be generated by a maneuver, in which case OSM verifies, in advance of its execution, the safety of the post-maneuver orbit. As a result, parameterizing the problem based on the one-orbit minimum RN distance makes it possible to check the safety criterion of Eq. (1) based on only two epochs (*i.e.*, the current and prediction

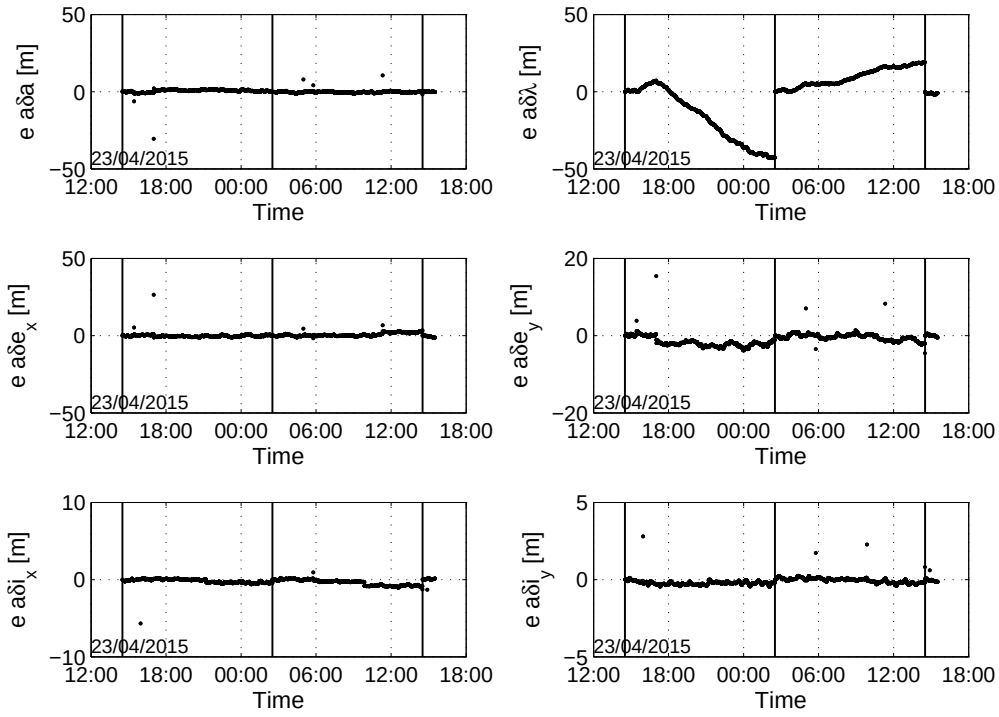

Figure 7. OSM propagation error.

times) in order to provide a reliable assessment valid over long-lasting periods of time. This last aspect is particularly convenient for onboard applications.

Figure 9 focuses on the RN plane. Here the lower bound of the minimum RN distance distribution is visualized as a circumference centered on the origin with radius $y - 3\sigma_y - M$.

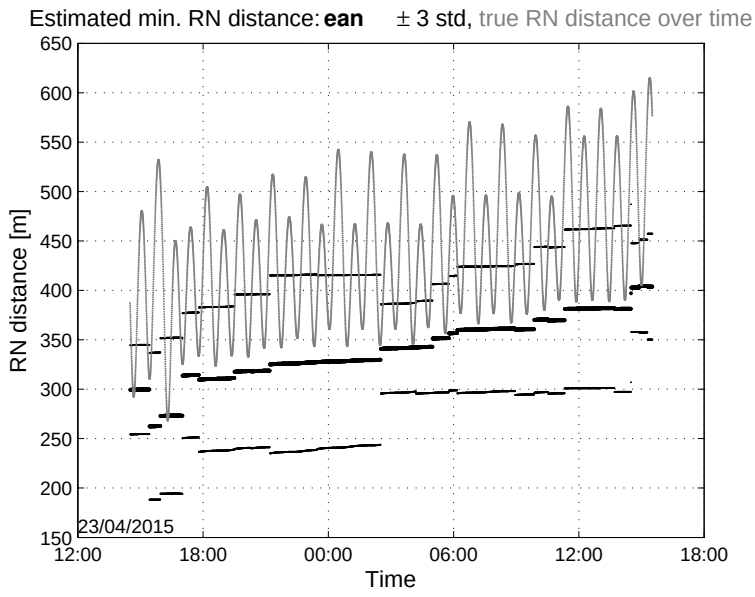

Figure 8. Superposition of the true RN distance over time (gray) and first two moments of the estimated minimum RN distribution (black).

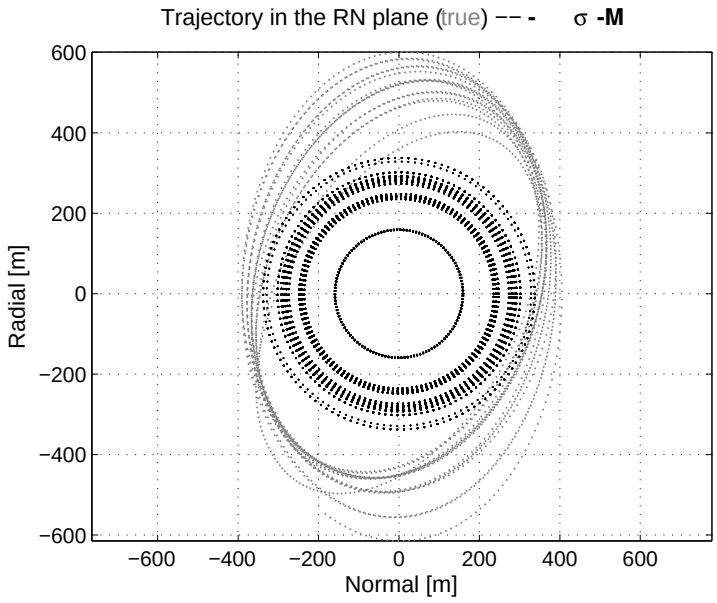

Figure 9. Superposition of the true RN trajectory (gray) and the estimated lower bound of the minimum RN distribution (black).

CONCLUSION

This paper presented the safety concept retained to monitor and guarantee the formation safety during the execution of the AVANTI experiment, which is an in-flight demonstration of vision-based proximity operations with respect to a noncooperative client satellite in low Earth orbit.

The peculiarity of the proposed approach is that it does not rely on the continuous real-time availability of tracking data of the client spacecraft but rather exploits the concept of passive safety of special relative trajectories. To this end, a formation safety criterion based on the characteristics of the uncertainty distribution of the minimum one-orbit distance normal to the flight direction has been defined.

In order to achieve a reliable and computationally light assessment of such safety criterion, the paper introduces the following novelties. First an analytical expression of the minimum one-orbit radial-normal distance applicable to the most general set of relative orbital elements is presented. This expression, in fact, allows extending the passive-safety concept to drifting relative orbits, resulting from a non-vanishing relative semi-major axis encountered during a rendezvous or produced by the action of the differential aerodynamic drag. Second, the unscented transformation framework is employed in order to achieve an accurate approximation of the relevant moments of the minimum distance distribution, generated by relative navigation and maneuver execution errors.

REFERENCES

[1] G. Gaias, J.-S. Ardaens, and S. D'Amico, "The Autonomous Vision Approach Navigation and Target Identification (AVANTI) Experiment: Objectives and Design," Porto, Portugal, 9th International ESA Conference on Guidance, Navigation & Control Systems, 2014.

[2] H. Reile, E. Lorenz, and T. Terzibaschian, "The FireBird Mission - A Scientific Mission for Earth Observation and Hot Spot Detection," *Small Satellites for Earth Observation, Digest of the 9th International Symposium of the International Academy of Astronautics*, Berlin, Germany, Wissenschaft und Technik Verlag, 2013. ISBN 978-3-89685-574-9.

[3] S. D'Amico, J.-S. Ardaens, and R. Larsson, "Spaceborne Autonomous Formation-Flying Experiment on the PRISMA Mission," *Journal of Guidance, Control, and Dynamics*, Vol. 35, No. 3, 2012, pp. 834–850. doi: 10.2514/1.55638.

[4] J.-S. Ardaens, S. D'Amico, and D. Fischer, "Early Flight Results from the TanDEM-X Autonomous Formation Flying System," St-Hubert, Quebec, 4th International Conference on Spacecraft Formation Flying Missions & Technologies (SFFMT), 2011.

[5] J.-S. Ardaens, R. Kahle, and D. Schulze, "In-Flight Performance Validation of the TanDEM-X Autonomous Formation Flying System," Munich, Germany, 5th International Conference on Spacecraft Formation Flying Missions & Technologies (SFFMT), 2013.

[6] T. Karlsson, N. Ahlgren, R. Faller, and B. Schlepp, "PRISMA Mission Control: Transferring Satellite Control between Organisations," Stockholm, Sweden, SpaceOps 2012, 2012.

[7] S. D'Amico, J.-S. Ardaens, G. Gaias, H. Benninghoff, B. Schlepp, and J. L. Jørgensen, "Noncooperative Rendezvous Using Angles-Only Optical Navigation: System Design and Flight Results," *Journal of Guidance, Control, and Dynamics*, Vol. 36, No. 6, 2013, pp. 1576–1595. doi: 10.2514/1.59236.

[8] P. Bodin, R. Noteborn, R. Larsson, T. Karlsson, S. D'Amico, J.-S. Ardaens, M. Delpech, and J. C. Berges, "PRISMA Formation Flying Demonstrator: Overview and Conclusions from the Nominal Mission," No. 12-072, Breckenridge, Colorado, USA, 35th Annual AAS Guidance and Control Conference, 2012.

[9] G. Gaias, J.-S. Ardaens, and O. Montenbruck, "Model of J2 Perturbed Satellite Relative Motion with Time-Varying Differential Drag," *Celestial Mechanics and Dynamical Astronomy*, Vol. 123, No. 4, 2015, pp. 411–433. doi: 10.1007/s10569-015-9643-2.

[10] J.-S. Ardaens and G. Gaias, "Spaceborne Autonomous Vision-Based Navigation System for AVANTI," Toronto, Canada, 65th International Astronautical Congress, 2014.

[11] G. Gaias, S. D'Amico, and J.-S. Ardaens, "Generalized Multi-Impulsive Maneuvers for Optimum Spacecraft Rendezvous in Near-Circular Orbit," *Int. J. Space Science and Engineering*, Vol. 3, No. 1, 2015, pp. 68–88. doi: 10.1504/IJSPACESE.2015.069361.

[12] A. Härting, C. K. Rajasingh, M. C. Eckstein, A. F. Leibold, and K. N. Srinivasamurthy, "On the collision hazard of colocated geostationary satellites," No. 88-4239, Minneapolis, USA, AIAA/AAS Astrodynamics conference, 1988.

[13] O. Montenbruck, M. Kirschner, S. D'Amico, and S. Bettadpur, "E/I-Vector Separation for Safe Switching of the GRACE Formation," *Aerospace Science and Technology*, Vol. 10, No. 7, 2006, pp. 628–635. doi: 10.1016/j.ast.2006.04.001.

[14] S. D'Amico and O. Montenbruck, "Proximity Operations of Formation Flying Spacecraft using an Eccentricity/Inclination Vector Separation," *Journal of Guidance, Control and Dynamics*, Vol. 29, No. 3, 2006, pp. 554–563. doi: 10.2514/1.15114.

[15] O. Montenbruck, R. Kahle, S. D'Amico, and J.-S. Ardaens, "Navigation and Control of the TanDEM-X Formation," *Journal of the Astronautical Sciences*, Vol. 56, No. 3, 2008, pp. 341–357.

[16] R. Larsson, J. Mueller, S. Thomas, B. Jakobsson, and P. Bodin, "Orbit Constellation Safety on the PRISMA In-Orbit Formation Flying Test Bed," *Proceedings of the 3rd International Symposium on Formation Flying, Missions and Technologies*, ESA SP-654, 2008.

[17] S. Weiß, F. Kempe, and K. Brieß, "GPS Tracking on the Three-Axis-Stabilized Picosatellite BEESAT-4," Würzburg, Germany, 2013. 7th Pico and Nano Satellite Workshop on Technology for Small Satellite Research.

[18] R. Kahle, M. Weigel, M. Kirschner, S. Spiridonova, E. Kahr, and K. Letsch, "Relative Navigation to Non-cooperative Targets in LEO: Achievable Accuracy from Radar Tracking Measurements," *Int. J. Space Science and Engineering*, Vol. 2, No. 1, 2014, pp. 81–95.

[19] M. Wermuth, G. Gaias, and S. D'Amico, "Safe Picosatellite Release from a Small Satellite Carrier," *Journal of Spacecraft and Rockets*, Vol. 52, No. 5, 2015, pp. 1338–1347. doi: 10.2514/1.A33036.

[20] S. J. Julier and J. K. Uhlmann, "Unscented filtering and nonlinear estimation," *Proceedings of the IEEE*, Vol. 92, Mar 2004, pp. 401–422, 10.1109/JPROC.2003.823141.